Self-Powered Human-Interactive Transparent Nanopaper Systems

Junwen Zhong,[†,§] Hongli Zhu,[‡,§] Qize Zhong,[†,§] Jiaqi Dai,[‡] Wenbo Li,[†] Soo-Hwan Jang,[‡] Yonggang Yao,[‡] Doug Henderson,[‡] Qiyi Hu,[†] Liangbing Hu,[*,‡] and Jun Zhou[*,†]

[†]Wuhan National Laboratory for Optoelectronics, and School of Optical and Electronic Information, Huazhong University of Science and Technology, Wuhan 430074, China and [‡]Department of Materials Science and Engineering, University of Maryland, College Park, Maryland 20742, United States. [§]J.Z., H.Z., and Q.Z. contributed equally to this work.

ABSTRACT Self-powered human-interactive but invisible electronics have many applications in anti-theft and anti-fake systems for human society. In this work, for the first time, we demonstrate a transparent paper-based, self-powered, and human-interactive flexible system. The system is based on an electrostatic induction mechanism with no extra power system appended. The self-powered, transparent paper device can be used for a transparent paper-based art anti-theft system in museums or for a smart mapping anti-fake system in precious packaging and documents, by virtue of the advantages of adding/removing freely, having no impairment on the appearance of the protected objects, and being easily mass manufactured. This initial study bridges the transparent nanopaper with a self-powered and human-interactive electronic system, paving the way for the development of smart transparent paper electronics.

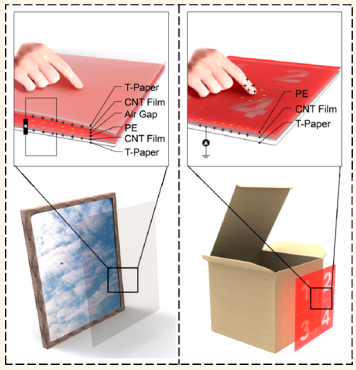

KEYWORDS: self-powered · anti-theft · anti-fake · transparent · paper-based

Paper electronics are not only highly flexible, light weight, eco-friendly, and low cost, but more importantly, these devices can be integrated easily into the regular paper system for origami and foldable electronics.[1−14] Transparent nanopaper (T-paper) made of transparent and strong nanocellulose is emerging as a promising substrate for flexible electronics due to its small surface roughness, tunable optical properties, good accessibility for functionalization, and excellent mechanical strength and flexibility.[15−17] Meanwhile, these nanopaper electronics are potentially biodegradable, biocompatible, and recyclable, which will minimize landfill problems.[18,19] So far, researchers have demonstrated transparent and flexible nanopaper transistors, organic light-emitting diodes (OLEDs), touch panels, antennas, *etc.*[15−19] However, all of the above-mentioned electronic devices require either external power sources or embedded batteries. It is important to establish self-powered paper electronic systems by accumulating environmental energy or converting body movement into electricity whenever and wherever possible.[20−26]

Meanwhile, a human-interactive electronic system, which can respond to human actions such as body movements and health parameters, is desired in various areas such as wearable electronics and mobile medication, *etc.* Smart self-powered and human-interactive electronics are meaningful for both consumer electronics, military, and defense electronics. Devices such as health/wellness monitors, body sensor networks, and artificial muscles have been reported recently.[27−32] Consequently, it is interesting and practical to bridge the T-paper with a self-powered and human-interactive electronic system and introduce a new developing direction for smart paper electronics.

Herein, we introduce a self-powered human-interactive transparent nanopaper system based on an electrostatic induction mechanism. Design, fabrication, and successful operation of the devices are clearly demonstrated. These devices show the following advantages: (1) they are self-powered, operating without the need for external power; (2) they are invisible, which is essential for anti-theft or anti-fake applications; (3) they are based on paper, which is compatible with other paper materials such as arts, packaging,

* Address correspondence to jun.zhou@mail.hust.edu.cn, binghu@umd.edu.

Received for review April 22, 2015 and accepted June 29, 2015.

Published online 10.1021/acsnano.5b02414

and documents; (4) they are sensitive to external pressure; (5) they can be added/removed freely and are easy for mass manufacturing. The human-interactive transparent nanopaper system could be potentially manufactured at a large scale for practical applications, such as anti-theft or anti-fake applications.

RESULTS AND DISCUSSION

Design of a Potential System Integration of Transparent Paper-Based Flexible Generator (TPFG). Due to the advantages of high transparency, excellent mechanical properties, and good compatibility, the TPFG can be utilized as a pressure sensor and assembled into a highly transparent paper-based art anti-theft system, as shown in Figure 1a. The transparent paper-based art anti-theft system will not affect the appearance of the art and is also sensitive for detecting external pressure. Additionally, the system is compatible with paper arts and can be added or removed freely. Furthermore, a four-pixel transparent paper-based smart mapping anti-fake system based on transparent nanopaper is also demonstrated, as indicated in Figure 1b. Touching a specific position of the transparent paper-based smart mapping anti-fake system will show coded information, such as a date, which may have a potential anti-fake application in the smart packaging of some important documents, such as wills and birth certificates. Moreover, it is suitable for mass manufacturing because of its simple structure and fabrication process. It must be noted that this work is a helpful step for building up the whole paper-based electronic systems by integrating it with other paper-based electronics.[33]

Fabrication and Physical Properties of a Transparent Paper-Based Flexible Generator. The self-powered human-interactive transparent nanopaper system is based on the TPFG. Supporting Information Figure S1 and Figure 1a introduce the fabrication process and device structure of the TPFG. The TPFG is composed of two transparent components, which are defined as the carbon nanotubes (CNTs)/T-paper and polyethylene (PE)/CNTs/T-paper. The fabricating process begins with an obtained transparent nanopaper, whose digital picture and scanning electron microscope (SEM) images are indicated in Figure 2a and inset image in Figure S1, respectively, followed by CNT deposition processing shown in Figure S1. The corresponding SEM image of CNTs/T-paper in Figure 2b reveals that percolated CNTs with lengths of tens of micrometers are deposited evenly on the transparent nanopaper surface. Additionally, Figure S2a,b illustrates the atomic force microscopy (AFM) images of the T-paper and CNTs/T-paper surface, respectively. Figure S2c clearly demonstrates that T-paper as well as CNTs/T-paper has nanoscale roughness, which will have little effect on the transmittance, that is, 95 and 93.5% in the visible region, respectively (Figure 2g). Furthermore, the nanoscale roughness will not affect the charge generation

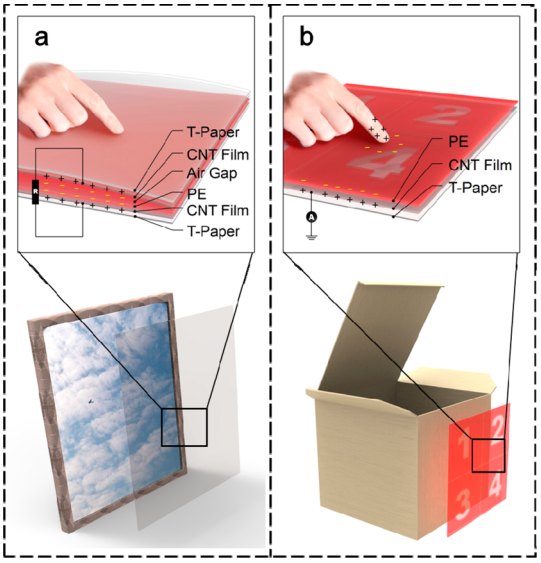

Figure 1. Schematic diagram for (a) transparent paper-based art anti-theft system and (b) transparent paper-based smart mapping anti-fake system. The transparent paper-based art anti-theft system may be applied to protect valuable art in museums, and the transparent paper-based smart mapping anti-fake system may have applications in smart packaging or important documents.

properties because the relief amplitude is less than 5 μm.[34] Deformation under various bending angles and durability tests were also carried out. During the measurement, the CNT electrode sheet resistance of $\sim$2 kΩ/cm^2 almost remained stable under various bending angles for the first bending, first recovery, and second bending process, as shown in Figure 2c,d. Simultaneously, the CNT electrode was continuously bent 1000 times under a 60° bending angle, and the $I-V$ curve remained almost the same (Figure 2e), which identified the good flexibility and stability of CNT electrodes on the transparent nanopaper surface. The above studies indicate that CNTs are excellent transparent electrodes for transparent nanopapers, with outstanding adhesion and conductivity.[15,35]

A $\sim$30 μm PE film was covered on the CNTs/T-paper to form the PE/CNTs/T-paper (Supporting Information Figure S1 and Figure 2f). Compared with a traditional fluoric electret, such as polytetrafluoroethylene (PTFE), PE is a transparent and non-fluorine electret and much more environmentally friendly. The surface morphology of the PE was characterized by AFM. The relative height of the surface was measured along the white line in Figure S2d. The height varied from $\sim$8 to $\sim$12 nm (Figure S2e). As discussed above, the nanoscale surface morphology has little effect on the transmittance rate that is maintained at more than 94% (Figure S2f). The long axis edges of the CNTs/T-paper and PE/CNTs/T-paper components were then adhered together, making the PE face the CNTs to form the TPFG. The transmittance of the TPFG remains above 90% within the visible light region, which could be

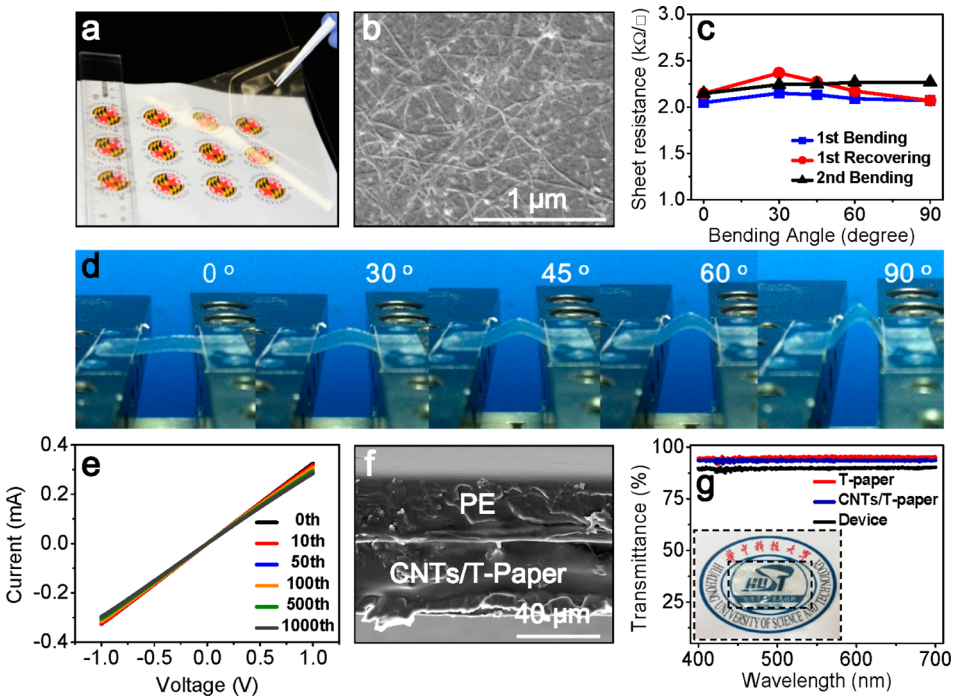

Figure 2. Physical properties of a TPFG. (a) Digital picture of transparent nanopaper. (b) SEM image of CNTs on the transparent nanopaper surface. (c) Sheet resistances of CNT electrodes under the first bending, first recovery, and second bending process. (d) Digital pictures of the CNTs/T-paper bent at different angles. (e) Durability test of CNT electrodes. (f) SEM image of the cross section view of the PE/CNTs/T-paper. (g) Transmittance of the transparent nanopaper, CNTs/T-paper, and TPFG; inset shows the digital picture of a TPFG.

attributed to the excellent transmittance of the unit component (Figure 2g and inset).

Working Mechanism Analysis. Electret generators to harvest energy have been reported previously, especially those used in the microelectromechanical systems (MEMS) field, where the fabrication is quite complex and most of the devices are solid.[35−37] In our study, the TPFG can be regarded as a parallel capacitor, ignoring that the edge effect and the fundamental working mechanism of the TPFG are electrostatic induction effects caused by the retaining charges. Since the PE film electret polarized by a corona method can be considered to be an electric field source,[14,38] achieving retaining charges (Q_P) of the PE film is quite necessary. The surface potential of the PE film monitored by an electrometer for nearly one month is investigated in Figure 3a, maintaining a narrow fluctuation near −550 V after several weeks of natural attenuation, clearly indicating the existence of Q_P. As a result, the Q_P will induce positive charges in the top PE/CNTs/T-paper component electrode (Q_T) and bottom CNTs/T-paper component electrode (Q_B) due to the electrostatic induction, where $-Q_P = Q_T + Q_B$.[38] Clearly, the significance of PE from the output current−time curves for the devices with and without PE can be seen in Figure 3b. The current amplitude of the device with PE is about 0.4 μA, but without PE, it is about 15 nA because there are almost no retaining charges for the device without the PE film.

In this work, the variation of the air gap between the two components has a key role in the generation of the alternating electric currents. When the TPFG is in the original state (Figure 3c-I), the TPFG is in the potential equilibrium state and no free electrons will flow in the external circuit. When the vertical compression is applied to the TPFG, the air gap becomes smaller. More positive charges will be induced in the bottom CNT electrode, leading to an increase of Q_B and a decrease of Q_T. As a result, the equilibrium state is broken and current will flow from the top CNT electrode to the bottom CNT electrode (Figure 3c-II). With the compression increasing, more positive charges are continually accumulated in the bottom CNT electrode until the potential distribution is in equilibrium (Figure 3c-III). In the releasing process, the air gap is increased, resulting in an increase of Q_T and a decrease of Q_B. In that case, currents will flow back to the top CNT electrode (Figure 3c-IV). The detailed potential distribution of the top and bottom electrodes is systematically simulated by the COMSOL Multiphysics software and is provided in the Supporting Information, Figure S3a and supporting calculation.

In general, the output performance of TPFG is related to the retaining charges (Q_P) of PE film and the air gap variation between the PE/CNTs/T-paper and CNTs/T-paper. Pressing and releasing the TPFG will produce alternating currents through the external circuit, which is shown in Figure 3d. Switching polarity tests were also carried out to confirm that the

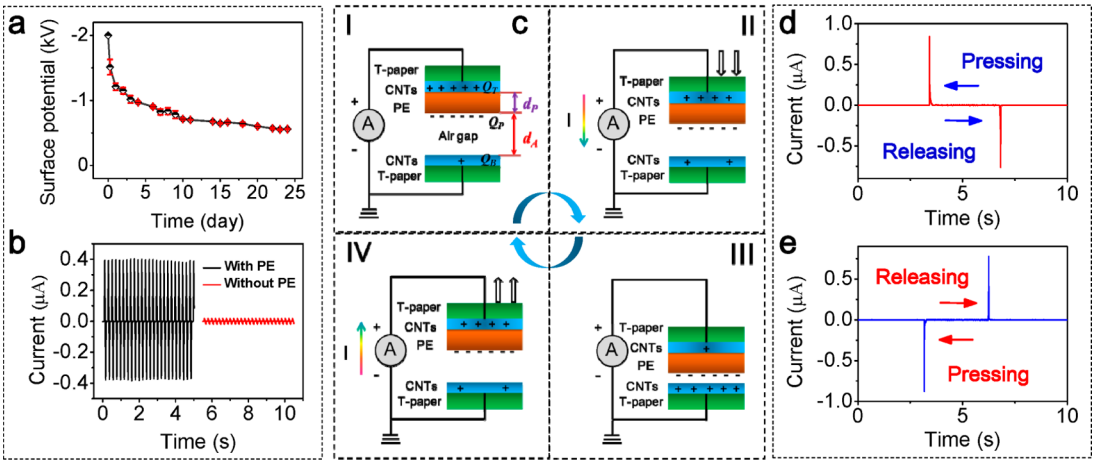

Figure 3. Working mechanism analysis of a TPFG. (a) Surface potential decay of the PE electret. (b) Output currents for the devices with and without PE electret. (c) Schematic diagram showing the working process of a TPFG when it is at (I) the original, (II) the pressing, (III) the equilibrium, and (IV) the releasing states. Corresponding short-circuit current−time curves for a TPFG when it is (d) forward-connected and (e) reverse-connected to the measurement system.

measured output signals are generated from the TPFG rather than from the measurement system (Figure 3e). Moreover, the open-circuit voltage of the TPFG was ~28 V, as shown in Figure S3. Furthermore, a theoretical analysis with its numerical solution is also carried out and shown in Supporting Information (Figure S4 and supporting calculation) to illustrate the working mechanism more mathematically.

Performance of Transparent Paper-Based Flexible Generator and Transparent Paper-Based Art Anti-theft System. The sensitive and stable output performances of the TPFG ensure its practical application. The typical electrical output performance of a TPFG with an effective area of 2×2 cm^2 was carefully studied by periodically pressing and releasing at controlled frequencies and amplitudes. Typically, a TPFG was attached to an elastic plastic sheet, one end of which was tightly fixed to an *x-y-z* mechanical stage, and the TPFG was periodically stimulated by a resonator. It should be noted that all of the electrical measurements were carried out after the surface potential of PE in a stable state. The output loading peak currents and corresponding loading peak power are shown in Figure S5. The stimulated amplitude and frequency are 2.5 mm and 5 Hz, respectively, showing that the maximum loading peak power value is 7.95 μW.

The load resistance of all the following measurements was 20 MΩ. The measurement results are systematically shown in Figure 4 and Supporting Information Figure S6. Under a given stimulated frequency of 5 Hz, the load peak currents of a generator increased approximately linearly as the stimulated amplitude increased from ~0.092 μA at 0.5 mm to 0.466 μA at 2.5 mm (Figure 4a). Meanwhile, the integral transferred charge curves corresponding to a pair of current signals generated by the pressing and releasing process are shown in Figure S6a. The integral transferred charges changed approximately linearly, too, from ~3.51 nC at 0.5 mm to ~10.54 nC at 2.5 mm, the same variation tendency with the loaded peak currents (Figure 4b).

On the other hand, for given stimulated amplitude of 2 mm, the load peak current changed approximately linearly from 0.095 μA at 1 Hz to 0.377 μA at 5 Hz, as shown in Figure 4c. However, the integral transferred charges remained almost constant at a value of ~8.9 nC, as shown in Figure S6b and Figure 4d. As discussed in our previous work, the higher stimulated frequency will lead to a faster charge transfer process, but the total amounts of transferred charges only relate to the relative position between the two components (Δd_A).[14,38] Consequently, a larger stimulated amplitude will result in a higher load peak current and larger transferred charges, but increasing the stimulated frequency only yields a higher load peak current. According to the above results, the integral transferred charges only relate to the stimulated amplitude, and thus the TPFG can be used as a pressure sensor by measuring the integral transferred charges.

The stability of the TPFG is a very important performance to ensure its applications. Herein, the TPFG was continuously operated for ~54 000 cycles at a stimulated amplitude of 2 mm and a frequency of 5 Hz. The outputs for different stimulated cycles are shown in Figure 4e and Supporting Information Figure S6c. Both the output load currents and corresponding integral transferred charges remained almost the same during the continuous measurement process, with a variation of only −0.79 to +0.83% for the integral transferred charges (Figure 4f). The high stability performance of the TPFG is attributed to the excellent mechanical properties of the whole device and the excellent electret properties of PE.

Because of the highly transparent property, the TPFG can be assembled into a highly transparent paper-based art anti-theft system to protect valuable

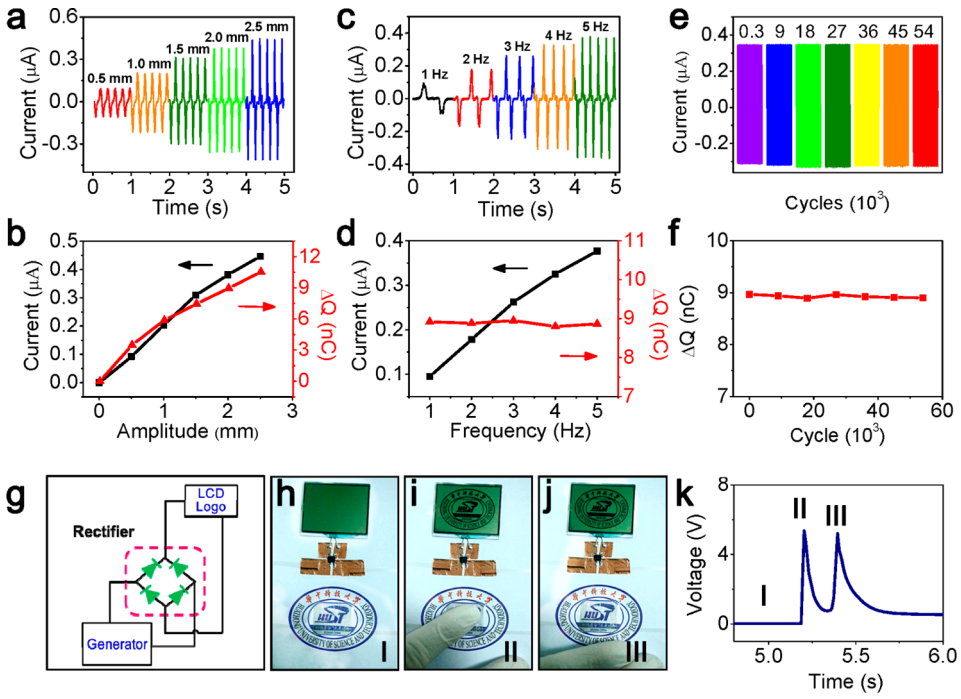

Figure 4. Performances of a TPFG and a transparent paper-based art anti-theft system. (a) Output current−time curves. (b) Load peak currents and corresponding transferred charges of a TPFG varied with stimulated amplitude of 0.5, 1, 1.5, 2, and 2.5 mm at a given frequency of 5 Hz. (c) Output current−time curves. (d) Load peak current and corresponding transferred charges of a TPFG varied with stimulate frequencies of 1, 2, 3, 4, and 5 Hz at a given amplitude of 2 mm. (e) Output current−time curves and (f) variation of corresponding transferred charges over time for ~54 000 continuous working cycles of a TPFG. (g) Equivalent circuit and (h) digital picture of a transparent paper-based art anti-theft system. Digital pictures show that the LCD logo was lit by (i) pressing motion and (j) releasing motion. (k) Corresponding voltage across the LCD logo when it was lit.

paper-based arts. As discussed above, the whole transparent paper-based art anti-theft system is fabricated with highly transparent materials, which will not impair the appearance of the paintings but will be sensitive to the pressure. Note that the device is invisible, which is an essential element for anti-theft applications. Figure 4g,h shows the circuit diagram and digital picture of a transparent paper-based art anti-theft system. When the TPFG was pressed and released, electric signals were generated. In order to improve the sensitivity, the alternating electric signals were first rectified by a bridge rectifier, so that both the pressing and releasing processes would trigger the alert (the liquid-crystal display (LCD) logo) (Figure 4i,j and Supporting Information video 1). As shown in Figure 4k, when the TPFG was being pressed or released, the voltage across the LCD was ~5.3 and ~5.1 V, respectively. The above results indicate that the transparent paper-based art anti-theft system can be integrated with paper-based products well and work effectively. It can be potentially applied for the protection of art in museums.

Performace of the Single-Electrode Transparent Paper-Based Smart Mapping Anti-fake System. To extend more self-powered human-interactive and responsive applications based on the T-paper, a single-electrode transparent smart mapping anti-fake system was demonstrated. The system is composed of a single piece of PE/CNTs/T-paper. In detail, four 1 × 1 cm^2 square CNT electrodes were deposited on a sheet of transparent nanopaper, leaving a 0.25 cm gap between them, and then a polarized PE film was adhered to the as-prepared transparent nanopaper. As a result, four independent single-electrode generators were assembled in one sheet of transparent nanopaper (Figures 1b and 5a). The working mechanism of the system is similar to the mechanism of the two-electrode generator discussed above. When an object such as a human finger approaches or leaves the PE electret film of the PE/CNTs/T-paper, the induced charges would emerge on the finger while the charges on the CNT electrode redistribute to balance an electrostatic equilibrium state. Consequently, charges will be transferred between the CNT electrode and the ground, generating the current signals. In our test process, each pixel was connected with a load resistor of 20 MΩ to the ground. When a specific pixel was touched by a finger, only the corresponding current singles were generated, which indicates that the four pixels can work independently and that the touching position is accurately located. When a specific pixel was touched by a finger, the corresponding number on LCD was lit (Figure 5b−e and Supporting Information video 2). The above results indicate that the transparent paper-based smart mapping anti-fake system can be assembled with paper-based packaging products

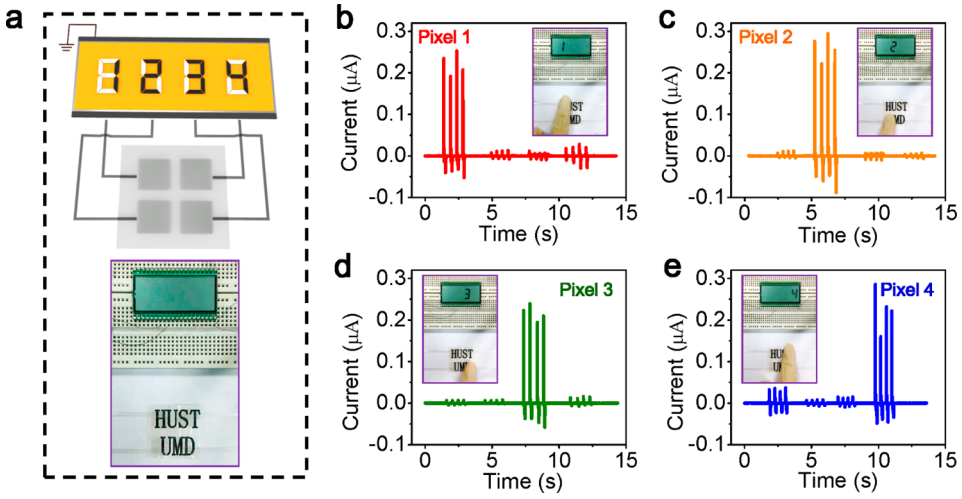

Figure 5. Performance of a transparent paper-based smart mapping anti-fake system. (a) Schematic diagram and digital picture of the transparent paper-based smart mapping anti-fake system. (b–e) Corresponding current singles for a specific pixel in the transparent paper-based smart mapping anti-fake system touched by a finger; inset is digital pictures showing the corresponding number lit on the LCD.

and may have potential applications in smart anti-fake systems. When a particular area of the transparent paper-based smart mapping anti-fake system is touched, coded information will be observed, such as brands and date. Touching different areas of the transparent paper-based smart mapping anti-fake system shows that different information may have a potential anti-fake application in the smart packaging or important documents, such as wills and birth certificates.

CONCLUSIONS

In summary, for the first time, we designed and demonstrated novel self-powered human-interactive transparent nanopaper systems, utilizing transparent nanopaper as base material. Highly transparent paper-based flexible generators were fabricated, and the working mechanism was thoroughly studied. The TPFG can be assembled into a highly transparent paper-based art anti-theft system, which can be integrated with valuable art in museums to protect the art. Attributed to the excellent transmittance, the protection system will not impact the appearance of the art. Meanwhile, the protection system can be added or removed freely. Moreover, a highly transparent paper-based smart mapping anti-fake system was also proposed. The transparent paper-based smart mapping anti-fake system has the ability to show coded and mapping information, indicating its potential as an anti-fake application in the smart packaging or for important documents, such as wills and birth certificates. This interesting smart transparent paper work may pave the way to self-powered, paper-based, and human-interactive electronics.

EXPERIMENTAL SECTION

Fabrication of T-Paper and CNTs/T-Paper. An aqueous nanofibrillated cellulose (NFC) dispersion was prepared from Southern Yellow Pine fibers according to a method previously reported by Zhu *et al.* Specifically, 78 mg of (2,2,6,6-tetramethylpiperidin-1-yl)oxyl (TEMPO) was subjected to ultrasonication in 100 mL of deionized (DI) water for 10 min to achieve a uniform solution, and then the TEMPO solution was combined with 514 mg of sodium bromide (NaBr) and dissolved in 50 mL of DI water. The TEMPO/NaBr mixture was then added to 5 g dry weight Kraft bleached softwood pulp suspended in 65 g of DI water. The TEMPO-mediated oxidation of the cellulose slurry was started by adding 30 mL of NaClO at room temperature. The pH was controlled at 10.5 by adjusting with 0.5 M NaOH solution. The pH was monitored every 20 min for 2 h. Once the TEMPO treatment was finished, the fibrous TEMPO-oxidized product was washed with water using Büchner filtration until white. Then the TEMPO-oxidized pulp was dispersed in water at a concentration of 1 wt % and disintegrated by one pass through a microfluidizer processor (M110 EH, Microfluidics Inc., USA). The treated wood pulp was pumped once through thin *z*-shaped chambers with channel dimension of 200 μm in the microfluidizer under a process pressure of 25 000 psi. A 1 wt % dispersion of NFC in water was obtained.

The NFC dispersion was then diluted with DI water and mixed at 500 rpm for 10 min. The final NFC dispersion had a concentration of 0.2 wt %. The dispersion was degassed for 20 min and poured through a nitrocellulose ester filter membrane with a pore size of 0.65 μm to obtain a transparent nanopaper. A thin layer of single-walled carbon nanotubes (SWNTs) was deposited on the transparent nanopaper surface *via* Aztek ultimate metal airbrush spray with nozzle #5 (TCP Corp., USA).

Fabrication of PE/CNTs/T-Paper. The CNTs/T-paper was cut to the size of 2 × 2 cm. Then PE film with a thickness of ~30 μm was covered on the CNTs/T-paper with the poly(ethylene oxide) (PEO) as the adhesive to form the PE/CNTs/T-paper. The PE electret was polarized in the direction perpendicular to it *via* the corona method under −15 kV high voltages for 5 min.

Fabrication of TPFG. The CNTs/T-paper and PE/CNTs/T-paper components were assembled to fabricate the TPFG. Specifically, the PE side of the PE/CNTs/T-paper was faced to the CNT side of the CNTs/T-paper, and then the edges of the two components were adhered together, forming an arch-shaped device.

Fabrication of Transparent Paper-Based Smart Mapping Anti-fake System. Four 1 × 1 cm^2 CNT electrodes were deposited on a sheet of transparent nanopaper, leaving a 0.25 cm gap between them, and then a polarized PE film was adhered to the as-prepared transparent nanopaper.

Characterization. The morphology of the samples was probed by a high-resolution field emission scanning electron microscope (FEI Nova Nano SEM 450) and atomic force microscope (AFM Dimension 3100 Veeco). The conductance of the CNT electrode was studied by Keithley 2400 sourcemeter. The transmittance of the samples was measured by a UV 2550 spectrophotometer (Shimadzu). The corona polarization method was carried out with DW-N503-4ACDE high-voltage source. The surface potential of the samples was detected by an electrometer (EST102, Huajing Beijing, China). A periodic stretching−releasing process of the samples was stimulated by a resonator (JZK, Sinocera, China), which was controlled by a sweep signal generator (YE 1311-D, Sinocera, China). The output of the samples was measured by a Stanford low-noise current preamplifier (model SR570) and NI PCI-6259.

Conflict of Interest: The authors declare no competing financial interest.

Supporting Information Available: More detailed information about calculation, detailed device fabrication process, supporting figures, and videos 1−3. The Supporting Information is available free of charge on the ACS Publications website at DOI: 10.1021/acsnano.5b02414.

Acknowledgment. J.Z. acknowledges the support from the National Natural Science Foundation of China (51322210, 61434001) and Director Fund of WNLO. L.H. acknowledges support from the DOD (Air Force of Scientific Research) Young Investigator Program. The authors thank the Center for Nanoscale Characterization & Devices for facility support, and WNLO-HUST and the Analysis and Testing Center of Huazhong University of Science and Technology.

REFERENCES AND NOTES

1. Granmar, M.; Cho, A. Electronic Paper: A Revolution About to Unfold? *Science* **2005**, *308*, 785–786.
2. Martins, R.; Nathan, A.; Barros, R.; Pereira, L.; Barquinha, P.; Correia, N.; Costa, R.; Ahnood, A.; Ferreira, I.; Fortunato, E. Complementary Metal Oxide Semiconductor Technology with and on Paper. *Adv. Mater.* **2011**, *23*, 4491–4496.
3. Russo, A.; Ahn, B. Y.; Adams, J. J.; Duoss, E. B.; Bernhard, J. T.; Lewis, J. A. Pen-on-Paper Flexible Electronics. *Adv. Mater.* **2011**, *23*, 3426–3430.
4. Eder, F.; Klauk, H.; Halik, M.; Zschieschang, U.; Schmid, G.; Dehm, C. Organic Electronics on Paper. *Appl. Phys. Lett.* **2004**, *84*, 2673–2675.
5. Berggren, M.; Nilsson, D.; Robinson, N. Organic Materials for Printed Electronics. *Nat. Mater.* **2007**, *6*, 3–5.
6. Yuan, L.; Xiao, X.; Ding, T.; Zhong, J.; Zhang, X.; Shen, Y.; Hu, B.; Huang, Y.; Zhou, J.; Wang, Z. L. Paper-Based Supercapacitors for Self-Powered Nanosystems. *Angew. Chem., Int. Ed.* **2012**, *51*, 4934–4938.
7. Johnson, R.; Evans, J.; Jacobsen, P.; Thompson, J.; Christopher, M. The Changing Automotive Environment: High-Temperature Electronics. *IEEE Trans. Electron. Packag. Manuf.* **2004**, *27*, 164–176.
8. Fan, Z.; Arunasalam, P.; Murray, B.; Sammakia, B. Modeling Heat Transport in Thermal Interface Materials Enhanced with MEMS-Based Microinterconnects. *IEEE Trans. Compon. Packag. Technol.* **2010**, *33*, 16–24.
9. Liu, J.; Yang, C.; Wu, H.; Lin, Z.; Zhang, Z.; Wang, R.; Li, B.; Kang, F.; Shi, L.; Wong, C. P. Future Paper Based Printed Circuit Boards for Green Electronics: Fabrication and Life Cycle Assessment. *Energy Environ. Sci.* **2014**, *7*, 3674–3682.
10. Grau, G.; Kitsomboonloha, R.; Swisher, S. L.; Kang, H.; Subramanian, V. Printed Transistors on Paper: Towards Smart Consumer Product Packaging. *Adv. Funct. Mater.* **2014**, *24*, 5067–5074.
11. Kim, K.-H.; Lee, K. Y.; Seo, J.-S.; Kumar, B.; Kim, S.-W. Paper-Based Piezoelectric Nanogenerators with High Thermal Stability. *Small* **2011**, *7*, 2577–2580.
12. Dauner, J.; Karagozler, M.; Poupyrev, I. Paper Generators: Harvesting Energy from Touching, Rubbing and Sliding. In *Proceedings of the 26th Annual ACM Symposium on User Interface Software and Technology*; St. Andrews, U.K., October 8−11, 2013; ACM: New York, 2013; pp 23−30.
13. Zhang, L.; Xue, F.; Du, W.; Han, C.; Zhang, C.; Wang, Z. Transparent Paper-Based Triboelectric Nanogenerator as A Page Mark and Anti-Theft Sensor. *Nano Res.* **2014**, *7*, 1215–1223.
14. Zhong, Q.; Zhong, J.; Hu, B.; Hu, Q.; Zhou, J.; Wang, Z. L. A Paper-Based Nanogenerator as A Power Source and Active Sensor. *Energy Environ. Sci.* **2013**, *6*, 1779–1784.
15. Huang, J.; Zhu, H.; Chen, Y.; Preston, C.; Rohrbach, K.; Cumings, J.; Hu, L. Highly Transparent and Flexible Nanopaper Transistors. *ACS Nano* **2013**, *7*, 2106–2113.
16. Grau, G.; Kitsomboonloha, R.; Swisher, S. L.; Kang, H.; Subramanian, V. Printed Transistors on Paper: Towards Smart Consumer Product Packaging. *Adv. Funct. Mater.* **2014**, *24*, 5067–5074.
17. Fang, Z.; Zhu, H.; Yuan, Y.; Ha, D.; Zhu, S.; Preston, C.; Chen, Q.; Li, Y.; Han, X.; Lee, S.; et al. Novel Nanostructured Paper with Ultrahigh Transparency and Ultrahigh Haze for Solar Cells. *Nano Lett.* **2014**, *14*, 765–773.
18. Zhu, H.; Xiao, Z.; Liu, D.; Li, Y.; Weadock, N. J.; Fang, Z.; Huang, J.; Hu, L. Biodegradable Transparent Substrates for Flexible Organic-Light-Emitting Diodes. *Energy Environ. Sci.* **2013**, *6*, 2105–2111.
19. Zhu, H.; Narakathu, B. B.; Fang, Z.; Tausif Aijazi, A.; Joyce, M.; Atashbar, M.; Hu, L. A Gravure Printed Antenna on Shape-Stable Transparent Nanopaper. *Nanoscale* **2014**, *6*, 9110–9115.
20. Xu, S.; Hansen, B. J.; Wang, Z. L. Piezoelectric-Nanowire-Enabled Power Source for Driving Wireless Microelectronics. *Nat. Commun.* **2010**, *1*, 93.
21. Zhu, G.; Chen, J.; Zhang, T.; Jing, Q.; Wang, Z. L. Radial-Arrayed Rotary Electrification for High Performance Triboelectric Generator. *Nat. Commun.* **2014**, *5*, 3426.
22. Bae, J.; Lee, J.; Kim, S.; Ha, J.; Lee, B.-S.; Park, Y.; Choong, C.; Kim, J.-B.; Wang, Z. L.; Kim, H.-Y.; Park, J.-J.; Chung, U. I. Flutter-Driven Triboelectrification for Harvesting Wind Energy. *Nat. Commun.* **2014**, *5*, 4929.
23. Fan, F. R.; Tian, Z. Q.; Wang, Z. L. Flexible Triboelectric Generator. *Nano Energy* **2012**, *1*, 328–334.
24. Moon, J. K.; Jeong, J.; Lee, D.; Pak, H. K. Electrical Power Generation by Mechanically Modulating Electrical Double Layers. *Nat. Commun.* **2013**, *4*, 1487.
25. Fan, X.; Chen, J.; Yang, J.; Bai, P.; Li, Z.; Wang, Z. L. Ultrathin, Rollable, Paper-Based Triboelectric Nanogenerator for Acoustic Energy Harvesting and Self-Powered Sound Recording. *ACS Nano* **2015**, *9*, 4236.
26. Yang, P. K.; Lin, Z. H.; Pradel, K. C.; Lin, L.; Li, X.; Wen, X.; He, J.-H.; Wang, Z. L. Paper-Based Origami Triboelectric Nanogenerators and Self-Powered Pressure Sensors. *ACS Nano* **2015**, *9*, 901–907.
27. Zhong, J.; Zhang, Y.; Zhong, Q.; Hu, Q.; Hu, B.; Wang, Z. L.; Zhou, J. Fiber-Based Generator for Wearable Electronics and Mobile Medication. *ACS Nano* **2014**, *8*, 6273–6280.
28. Lee, J. A.; Shin, M. K.; Kim, S. H.; Cho, H. U.; Spinks, G. M.; Wallace, G. G.; Lima, M. D.; Lepró, X.; Kozlov, M. E.; Baughman, R. H.; et al. Ultrafast Charge and Discharge Biscrolled Yarn Supercapacitors for Textiles and Microdevices. *Nat. Commun.* **2013**, *4*, 2979.
29. Zeng, W.; Shu, L.; Li, Q.; Chen, S.; Wang, F.; Tao, X.-M. Fiber-Based Wearable Electronics: A Review of Materials, Fabrication, Devices, and Applications. *Adv. Mater.* **2014**, *26*, 5310–5336.
30. Gong, S.; Schwalb, W.; Wang, Y.; Chen, Y.; Tang, Y.; Si, J.; Shirinzadeh, B.; Cheng, W. A Wearable and Highly Sensitive Pressure Sensor with Ultrathin Gold Nanowires. *Nat. Commun.* **2014**, *5*, 4132.
31. Kim, S. J.; We, J. H.; Cho, B. J. A Wearable Thermoelectric Generator Fabricated on A Glass Fabric. *Energy Environ. Sci.* **2014**, *7*, 1959–1965.

32. Yang, J.; Chen, J.; Liu, Y.; Yang, W.; Su, Y.; Wang, Z. L. Triboelectrification-Based Organic Film Nanogenerator for Acoustic Energy Harvesting and Self-Powered Active Acoustic Sensing. *ACS Nano* **2014**, *8*, 2649–2657.
33. Lien, D.-H.; Kao, Z.-K.; Huang, T.-H.; Liao, Y.-C.; Lee, S.-C.; He, J.-H. All-Printed Paper Memory. *ACS Nano* **2014**, *8*, 7613–7619.
34. Fan, F.-R.; Lin, L.; Zhu, G.; Wu, W.; Zhang, R.; Wang, Z. L. Transparent Triboelectric Nanogenerators and Self-Powered Pressure Sensors Based on Micropatterned Plastic Films. *Nano Lett.* **2012**, *12*, 3109–3114.
35. Xu, W. J.; Kranz, M.; Kim, S. H.; Allen, M. G. Micropatternable Elastic Electrets Based on A PDMS/Carbon Nanotube Composite. *J. Micromech. Microeng.* **2010**, *20*, 104003.
36. Mitcheson, P. D.; Miao, P.; Stark, B. H.; Yeatman, E. M.; Holmes, A. S.; Green, T. C. MEMS Electrostatic Micropower Generator for Low Frequency Operation. *Sens. Actuators, A* **2004**, *115*, 523–529.
37. Suzuki, Y.; Miki, D.; Edamoto, M.; Honzumi, M. A MEMS Electret Generator with Electrostatic Levitation for Vibration-Driven Energy-Harvesting Applications. *J. Micromech. Microeng.* **2010**, *20*, 104002.
38. Zhong, J.; Zhong, Q.; Fan, F.; Zhang, Y.; Wang, S.; Hu, B.; Wang, Z. L.; Zhou, J. Finger Typing Driven Triboelectric Nanogenerator and Its Use for Instantaneously Lighting up LEDs. *Nano Energy* **2013**, *2*, 491–497.